Defining mechanisms of actin polymerization and depolymerization during dendritic spine morphogenesis

Pirta Hotulainen,[1,2] Olaya Llano,[1] Sergei Smirnov,[1] Kimmo Tanhuanpää,[1] Jan Faix,[3] Claudio Rivera,[1] and Pekka Lappalainen[1,2]

[1]Institute of Biotechnology and [2]Neuroscience Center, University of Helsinki, Helsinki FI-00014, Finland
[3]Institute for Biophysical Chemistry, Hannover Medical School, Hannover D-30623, Germany

Dendritic spines are small protrusions along dendrites where the postsynaptic components of most excitatory synapses reside in the mature brain. Morphological changes in these actin-rich structures are associated with learning and memory formation. Despite the pivotal role of the actin cytoskeleton in spine morphogenesis, little is known about the mechanisms regulating actin filament polymerization and depolymerization in dendritic spines. We show that the filopodia-like precursors of dendritic spines elongate through actin polymerization at both the filopodia tip and root. The small GTPase Rif and its effector mDia2 formin play a central role in regulating actin dynamics during filopodia elongation. Actin filament nucleation through the Arp2/3 complex subsequently promotes spine head expansion, and ADF/cofilin-induced actin filament disassembly is required to maintain proper spine length and morphology. Finally, we show that perturbation of these key steps in actin dynamics results in altered synaptic transmission.

Introduction

Dendritic spines, small actin-rich protrusions from dendritic shafts, are the primary locus of excitatory synapses on neurons. Changes in dendritic spine morphology play a key role in memory formation and learning (Kasai et al., 2003). The loss or malformation of spines is also linked to many neurological diseases, which indicates the importance of proper regulation of spine morphology (Calabrese et al., 2006). Spines come in a wide range of sizes and shapes, even within the same brain region and the same dendrite. Individual spines also change shape continuously. Developmental shape changes follow a progressive replacement of the thin, elongated, and highly motile filopodia-like structures by more stable dendritic spines, which reach morphological maturity with a distinct neck and head (Oray et al., 2006).

The actin cytoskeleton is central to numerous cellular processes involving membrane dynamics such as motility, morphogenesis, and endocytosis. During these processes, the barbed ends of polymerizing actin filaments push the membrane and promote the formation of plasma membrane protrusions or invaginations (Pollard and Borisy, 2003; Kaksonen et al., 2006;

Carlier and Pantaloni, 2007). The actin cytoskeleton also plays a pivotal role in dendritic spine morphogenesis and dynamics (Ethell and Pasquale, 2005; Sekino et al., 2007; Zhang and Macara, 2008).

Numerous actin-binding proteins under the control of different signaling pathways strictly regulate the dynamics of actin filaments, but information about the role of these proteins in dendritic spine morphogenesis is limited. The Arp2/3 complex is probably the most thoroughly characterized actin regulator in spine morphogenesis. Arp2/3 promotes nucleation of a branched actin filament network in other cell types (Pollard and Borisy, 2003; Pollard, 2007), and its expression is important for spine and synapse density (Wegner et al., 2008). Furthermore, reduced expression of its regulators affects spine morphology (Grove et al., 2004; Kim et al., 2006; Proepper et al., 2007; Soderling et al., 2007). Although these studies suggest that Arp2/3 complex induces formation of the branched actin network in the bulbous spine head, experimental evidence is still lacking.

Correspondence to Pirta Hotulainen: pirta.hotulainen@helsinki.fi

Abbreviations used in this paper: ADF, actin-depolymerizing factor; DIV, days in vitro; mEPSC, miniature excitatory postsynaptic current; V-GLUT-1, vesicular glutamate transporter 1.

The Rockefeller University Press $30.00
J. Cell Biol. Vol. 185 No. 2 323–339
www.jcb.org/cgi/doi/10.1083/jcb.200809046

JCB **323**

In addition to Arp2/3, the formin family actin-nucleating proteins are critical to formation of plasma membrane protrusions in other cell types. Formins typically promote formation of unbranched actin filaments (Goode and Eck, 2007). Electron microscopy studies suggested a branched actin filament network in spine heads but unbranched actin filaments in dendritic filopodia and spine necks (Fifková and Delay, 1982; Landis and Reese, 1983; Hirokawa, 1989). Formins are thus good candidates for proteins regulating the nucleation/polymerization of actin filaments in dendritic filopodia.

Actin-depolymerizing factor (ADF)/cofilins, which sever and depolymerize aged actin filaments, are also central regulators of cytoskeletal dynamics in many cell types (Bamburg, 1999). Two ADF/cofilin isoforms occur in the vertebrate central nervous system (Vartiainen et al., 2002), and they localize within the postsynaptic density in dendritic spines (Racz and Weinberg, 2006). LIM kinases, which inhibit actin filament disassembly by phosphorylating ADF/cofilins, are necessary for normal spine development (Meng et al., 2002, 2004). However, in addition to ADF/cofilins, LIM kinases do have other substrates, such as transcription factors CREB and Nurr1 (Yang et al., 2004; Sacchetti et al., 2006). Furthermore, ADF/cofilin phosphorylation is related to the formation of long-term potentiation and increased spine head volume (Fukazawa et al., 2003; Chen et al., 2007; Fedulov et al., 2007); correspondingly, ADF/cofilin dephosphorylation has been linked to long-term depression and spine shrinkage (Zhou et al., 2004). These data suggest that ADF/cofilins may be central to dendritic spine morphogenesis and dynamics.

Here, we identified the sites of actin filament assembly in filopodia-like spine precursors and in more mature spines. Furthermore, we revealed the roles of Arp2/3- and mDia2-induced actin filament nucleation and ADF/cofilin-induced actin filament disassembly in dendritic spine development and maintenance of correct spine morphology, as well as in synaptic activity. Based on these data, we propose a working model for regulation of dendritic spine morphogenesis by coordinated actin filament nucleation/polymerization and disassembly.

Results

To examine actin dynamics in dendritic spines, hippocampal neurons were cultured for 7, 13, or 20 d and transfected with a construct expressing GFP–β-actin (Choidas et al., 1998). Imaging was performed 1 d after transfection. Only cells expressing low to moderate amounts of GFP-actin were selected for further analysis. In all experiments, transfected cells grew in a dense network of neurons, ensuring the availability of a proper synaptic network and excluding differences in spine morphologies resulting from different cell densities.

As described previously (Takahashi et al., 2003; Oray et al., 2006), hippocampal neurons presented typical morphological changes, starting from filopodia-like protrusions (8 d in vitro [DIV]), progressing to spines with a reasonably long neck and small head (DIV 14), and finally changing to spines with a short neck and a large bulbous head (DIV 21; Fig. S1, A–C; and Videos 1 and 2). Rapid changes from filopodia-like to mushroom-shaped morphology were detected in DIV 14 neurons

(Fig. S1 D and Video 3). However, these changes were not permanent, and "stabilization" of mature morphology required a longer time. During all developmental stages, rapid changes in the actin cytoskeleton were obvious, and increased actin intensity typically preceded changes in spine morphology (Fig. S1 E and Video 4). These observations and earlier studies (Honkura et al., 2008; Okamoto et al., 2004) indicate that the localized actin polymerization against the dendritic plasma membrane may provide mechanical force for the morphological changes of spinogenesis.

Polymerization of actin filaments in dendritic filopodia

To reveal the sites of actin polymerization in dendritic filopodia, we first identified the cellular regions that are rich in free filament barbed ends. Polymerizing barbed ends concentrated at the tips of dendritic filopodia, as expected based on fibroblast filopodia (Gupton and Gertler, 2007; Mattila and Lappalainen, 2008), but surprisingly, they were also present in filopodia roots (Fig. 1, A–C). Polymerization sites were further confirmed by FRAP analysis, which revealed that GFP-actin monomers mainly incorporated at the filopodia tips (Fig. 1 D). However, in ∼10% of dendritic filopodia, fluorescence recovery was also detected at the root (Fig. 1 E). The tip and root recovery did not exclude each other; both types of recovery could occur in the same dendrite and even in the same filopodium (Fig. 1 E). Thus, unlike canonical filopodia, dendritic filopodia-like protrusions can contain polymerization-competent filament barbed ends at both tips and roots.

Two small Rho family GTPases, Cdc42 and Rif, regulate fibroblast filopodia formation (Faix and Rottner, 2006; Gupton and Gertler, 2007). We first expressed active (continuously in GTP form) and inactive (continuously in GDP form) Cdc42 (Vartiainen et al., 2000) and Rif (Ellis and Mellor, 2000) in DIV 12–13 hippocampal neurons. Cdc42 appeared to have a negative effect on filopodia formation, as expression of inactive Cdc42 increased the number of dendritic filopodia, whereas active Cdc42 had an opposite effect (Tables I and II, and Fig. S2). Furthermore, expression of active Cdc42 increased the number of mushroom and stubby spines, and the width of spine heads was greater compared with wild-type neurons, suggesting that Cdc42 positively regulates spine head formation (Tables I–III, and Fig. S2). Interestingly, expression of inactive Rif resulted in a clear reduction in the number of dendritic filopodia and thin spines, whereas the number of mushroom and stubby spines increased (Fig. 2 A, C). The mean widths of the head regions of both thin and mushroom spines were also significantly increased (Table III). Dendritic protrusion length was slightly reduced, whereas the dendritic protrusion density was not significantly changed (Fig. 2, A and B; and Table IV). Active Rif did not induce significant changes in dendritic protrusion morphology or length, but dendritic protrusion density was decreased (Fig. 2, A, D, and E). These results indicate that Rif negatively regulates spine head expansion. As expression of inactive Rif also decreased the number of filopodia and mean length of dendritic protrusions, Rif may have a role in filopodia formation and elongation.
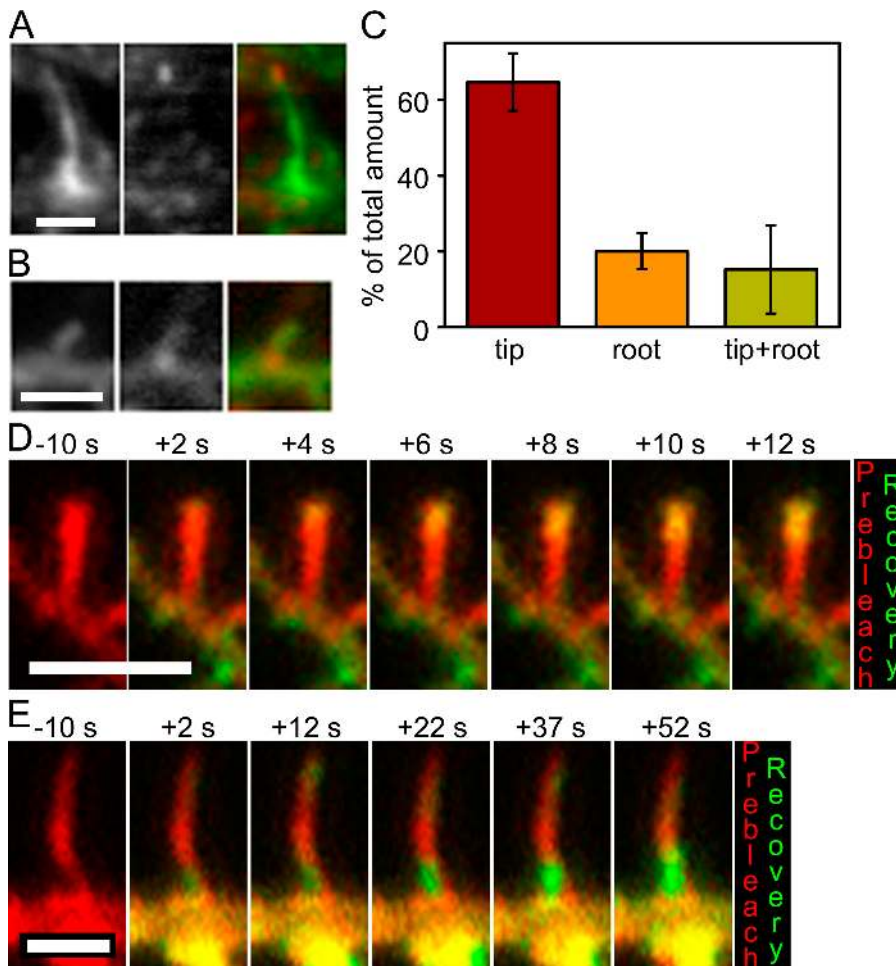
Figure 1. **Sites of actin filament polymerization in dendritic filopodia.** (A and B) The free actin filament barbed ends in mouse hippocampal neurons were visualized with fluorescently labeled actin monomers (middle panels). F-actin was stained with fluorescently labeled phalloidin (left panels). Right panels show merged images. The cell in A was fixed at DIV 16 and the cell in B was fixed at DIV 12. (C) The number of sites (percentage of total amount) of barbed ends in different locations (tip, root, or tip + root) was counted from 76 filopodia from four independent experiments (DIV 12–16). Data are presented as mean ± SEM. (D and E) Mouse cortical neurons were transfected with a construct expressing GFP–β-actin at DIV 8, and the FRAP assay was performed at DIV 9. GFP-actin was bleached from total filopodium (red), and the appearance of nonbleached actin (green) was followed by time-lapse imaging. In D, GFP-actin fluorescence recovers (actin filaments polymerize) from the filopodium tip; in E, recovery occurs mainly from the root. Bars, 1 µm.

The only effector of the Rif identified so far is the formin mDia2. In other cell types, mDia2 promotes filopodia formation by nucleation and elongation of actin filaments at filopodia tips (Pellegrin and Mellor, 2005; Schirenbeck et al., 2005; Kovar et al., 2006; Yang et al., 2007; Block et al., 2008). In accordance with previous work (Dent et al., 2007), we detected only low mDia2 protein levels during the early days in culture (DIV 7); however, mDia2 expression increased during the

Table I. **Density of filopodia, thin spines, mushroom spines, and stubby spines**

Description	n (neurons); DIV	Filopodia (mean ± SEM)	Thin spines (mean ± SEM)	Mushroom spines (mean ± SEM)	Stubby spines (mean ± SEM)
		μm^{-1}	μm^{-1}	μm^{-1}	μm^{-1}
GFP control	16; 12	0.18 ± 0.016	0.11 ± 0.014	0.038 ± 0.010	0.0096 ± 0.0031
Cdc42 GDP	15; 12	0.21 ± 0.028	0.017 ± 0.0042	0.013 ± 0.0044	0.018 ± 0.0059
Cdc42 GTP	17; 12	0.12 ± 0.016	0.024 ± 0.0060	0.039 ± 0.0073	0.054 ± 0.011
GFP control	16; 12	0.13 ± 0.016	0.090 ± 0.011	0.029 ± 0.0049	0.0097 ± 0.0026
Inactive Rif	18; 12	0.089 ± 0.0078	0.034 ± 0.0040	0.049 ± 0.0094	0.049 ± 0.0070
p34 siRNA	12; 12	0.14 ± 0.020	0.015 ± 0.0038	0.018 ± 0.0078	0.0065 ± 0.0017
cof1 siRNA	16; 12	0.12 ± 0.013	0.043 ± 0.0047	0.025 ± 0.0044	0.0060 ± 0.0016
cof1 siRNA + cof1-myc	14; 12	0.14 ± 0.017	0.12 ± 0.016	0.024 ± 0.0030	0.011 ± 0.0077
GFP control	14; 12	0.17 ± 0.016	0.091 ± 0.013	0.035 ± 0.0076	0.0058 ± 0.0019
Active Rif	18; 12	0.16 ± 0.016	0.058 ± 0.010	0.023 ± 0.0047	0.0056 ± 0.0010
GFP control	19; 12–13	0.16 ± 0.016	0.11 ± 0.011	0.030 ± 0.0051	0.0078 ± 0.0020
mDia2 siRNA	12; 12–13	0.11 ± 0.022	0.056 ± 0.013	0.031 ± 0.0046	0.017 ± 0.0040
GFP control	12; 12, and 14	0.17 ± 0.012	0.16 ± 0.022	0.027 ± 0.0056	0.015 ± 0.0045
Inactive Rif + active mDia2	12; 12, and 14	0.23 ± 0.032	0.011 ± 0.0070	0.012 ± 0.0059	0.015 ± 0.0091
GFP control	13; 12	0.18 ± 0.015	0.11 ± 0.014	0.037 ± 0.0057	0.0081 ± 0.0018
Inactive Rif + WA	18; 12	0.21 ± 0.021	0.019 ± 0.0058	0.0027 ± 0.0015	0.0030 ± 0.0017
W	14; 12	0.12 ± 0.016	0.093 ± 0.015	0.036 ± 0.0064	0.021 ± 0.0027
WA	15; 12	0.11 ± 0.015	0.011 ± 0.0025	0.0093 ± 0.0028	0.0068 ± 0.0019

Table II. **P-values for filopodium, thin spine, mushroom spine, and stubby spine densities presented in Table I**

Description	Filopodium	Thin spine	Mushroom spine	Stubby spine
Cdc42 GDP	0.453	**<0.001**	**0.015**	0.352
	0.016[a]	0.632[a]	**0.008**[a]	**0.010**[a]
Cdc42 GTP	**0.048**	**<0.001**	0.614	**<0.001**
Inactive Rif	0.084	**<0.001**	0.105	**<0.001**
p34 siRNA	0.577	**<0.001**	**0.025**	0.673
cof1 siRNA	0.940	**<0.001**	0.522	0.379
cof1 siRNA + cof1-myc	0.533	0.105	0.480	0.233
	0.533[b]	**<0.001**[b]	0.901[b]	0.515[b]
Active Rif	0.732	0.074	0.210	0.413
mDia2 siRNA	0.074	**0.002**	0.626	**0.018**
Inactive Rif + active mDia2	0.204	**<0.001**	0.050	0.208
Inactive Rif + WA	0.522	**<0.001**	**<0.001**	**0.008**
WA	0.458	**<0.001**	**<0.001**	**<0.001**

Statistically significant values (P < 0.050) are shown in bold.

[a]P-value for cdc42GDP:cdc42GTP.

[b]P-value for cof1 siRNA:cof1 siRNA + cof1 rescue.

development of spines, and the protein was clearly detectable at DIV 14 (Fig. S3 A). Active mDia2 localized to the tips of dendritic filopodia, the site of rapid actin filament polymerization (Figs. 1 and 3, A and B). Expression of the dominant-active mDia2 induced a loss of spine heads and formation of actin filament bundles along the dendrites (Fig. 3 A). Due to relatively modest expression levels of mDia2 from this plasmid and its accumulation to the tips of filopodia, the dendritic protrusion morphologies could not be reliably quantified from these cells. However, coexpression of inactive Rif with mDia2 allowed analysis of dendritic protrusion morphology. Co-expression of inactive Rif and active mDia2 induced a phenotype

similar to expression of active mDia2 alone (Fig. 3 B); the number of filopodia increased, and thin, mushroom, and stubby spines were almost totally lost (Fig. 3 D). This suggests that, similarly to HeLa cells and NIH 3T3 fibroblasts (Pellegrin and Mellor, 2005), Rif also regulates actin dynamics through mDia2 in hippocampal neurons (Fig. 3).

Next, we silenced mDia2 expression by RNAi. For this purpose, we used two different target sequences whose efficacy has been tested in nonneuronal cells, where high transfection efficiencies can be achieved. Sequence 1 was tested in mouse B16F1 fibroblasts (Yang et al., 2007), and sequence 2, which anneals with both mouse and human mRNA, was tested

Table III. **Spine head width**

Description	n (thin spines)	Thin spine (mean ± SEM)	P-value	n (mushroom)	Mushroom (mean ± SEM)	P-value
		μm			μm	
GFP control	247	0.51 ± 0.0079		64	0.96 ± 0.024	0.446
Cdc42 GDP	28	0.59 ± 0.018	**<0.001**	20	1.01 ± 0.058	0.275[a]
Cdc42 GTP	55	0.58 ± 0.014	0.836[a]	81	1.08 ± 0.032	**0.006**
			<0.001			
GFP control	263	0.54 ± 0.0077		81	0.92 ± 0.016	
Inactive Rif	78	0.58 ± 0.013	**<0.001**	99	1.06 ± 0.028	**0.001**
p34 siRNA	22	0.57 ± 0.035	0.261	18	0.93 ± 0.037	0.280
cof1 siRNA	134	0.56 ± 0.011	0.148	78	0.93 ± 0.018	0.778
cof1 siRNA + cof1 rescue	263	0.51 ± 0.0072	**0.016**	48	0.94 ± 0.026	0.897
			<0.001[b]			0.813[b]
GFP control	197	0.53 ± 0.0091	0.711	66	0.97 ± 0.025	0.182
Active Rif	102	0.54 ± 0.012		44	1.02 ± 0.035	
GFP control	320	0.52 ± 0.0073		84	0.93 ± 0.017	
mDia2 siRNA	85	0.56 ± 0.012	**0.001**	58	1.03 ± 0.026	**<0.001**
GFP control	225	0.48 ± 0.0087	0.678	37	0.94 ± 0.026	0.698
Inactive Rif + active mDia2	13	0.50 ± 0.046		16	0.97 ± 0.048	
GFP control	205	0.53 ± 0.0093	0.391	62	0.92 ± 0.021	0.271
Inactive Rif + WA	22	0.51 ± 0.023		4	0.97 ± 0.039	
W	174	0.58 ± 0.012	0.549	74	1.06 ± 0.025	0.736
WA	17	0.55 ± 0.040		20	1.07 ± 0.038	

Statistically significant values (P < 0.050) are shown in bold.

[a]P-value for cdc42GDP:cdc42GTP.

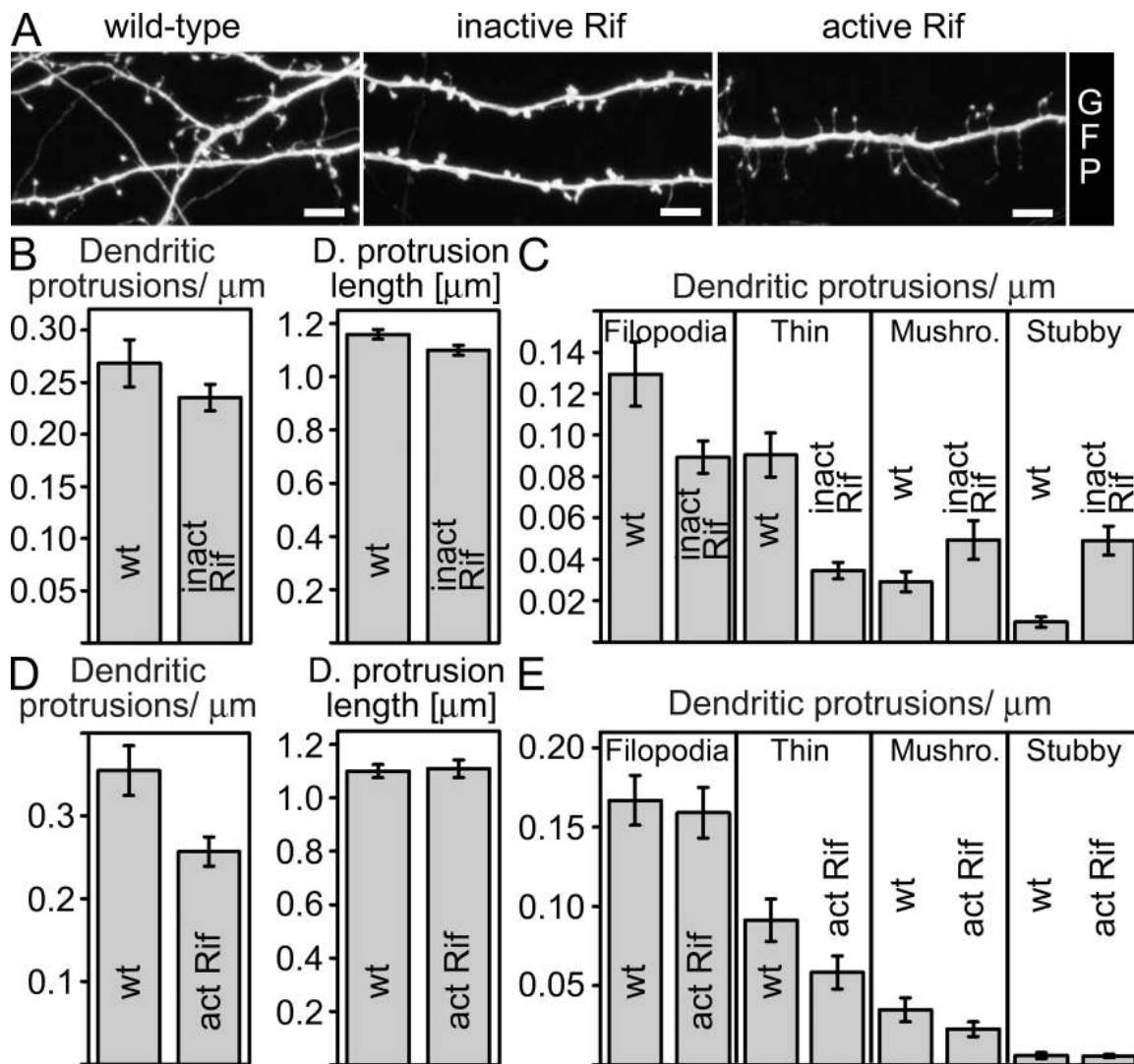[b]P-value for cof1 siRNA:cof1 siRNA + cof1 rescue.

Figure 2. **Role of Rif in spinogenesis.** (A) Mouse hippocampal neurons were transfected with GFP alone, or with GFP and myc-tagged inactive Rif or constitutively active Rif at DIV 11. Cells were fixed at DIV 12, and expression of Rif myc constructs was detected by anti-myc antibody (not depicted). Bars, 5 μm. (B) Quantitative analysis of neurons expressing inactive Rif (inact Rif) did not reveal significant changes in dendritic protrusion density as compared with wild-type cells (wt). Dendritic protrusion length was slightly reduced. Numerical data and p-values are presented in Table IV. (C) Dendritic protrusion morphology analysis of neurons expressing inactive Rif revealed a significant decrease in the number of thin spines and an increase in the number of stubby spines. Numerical data and p-values are presented in Tables I and II. (D) Quantitative dendritic protrusion analysis of neurons expressing active Rif (act Rif) revealed a significant reduction in dendritic protrusion density, whereas the mean length of dendritic protrusions was comparable to wild-type cells (wt). Numerical data are presented in Table IV. (E) Dendritic protrusion morphology analysis of neurons expressing active Rif did not reveal statistically significant changes between GFP and active Rif-transfected cells. Numerical data are shown in Tables I and II. Graphs represent mean ± SEM.

in human HeLa cells (unpublished data). The silencing efficacy in hippocampal neurons was determined by cotransfecting neurons with GFP and mDia2 siRNA followed by anti-mDia2 antibody immunofluorescence staining. mDia2 antibody staining intensity in the soma of GFP-expressing neurons was reduced by 54% compared with nontransfected neurons (Fig. S3, B and C). The reduced levels of mDia2 resulted in a decrease in the number of filopodia and thin spines but an increase in the number of stubby spines (Fig. 3, E and G). The mean spine head widths of thin and mushroom spines were significantly increased (Table III). Total dendritic protrusion density and dendritic protrusion length were decreased (Fig. 3 F). The same phenotype was achieved with both target sequences (sequence 1: Figs. 3 E and S3; and sequence 2: Video 5 [wild-type]

and Video 6 [mDia2 siRNA]), whereas transfecting cells with control siRNA oligonucleotides did not result in detectable changes in dendritic protrusion morphology (see Fig. 7 A and data not depicted).

The phenotype of mDia2 siRNA-treated cells closely resembled the one obtained by expressing inactive Rif (Fig. 2, A–C; and Fig. 3, E–G); however, the mDia2 siRNA-treated cells often displayed spines with more irregular morphology compared with those of cells expressing inactive Rif (Fig. 3 E). This might be due to fact that also Cdc42 can activate mDia2 (Peng et al., 2003); thus, when Rif is inhibited, mDia2 might be activated through another signaling route. It is also possible that Rif has other, currently unidentified effectors that regulate spine morphology. Together, these results suggest that Rif and its
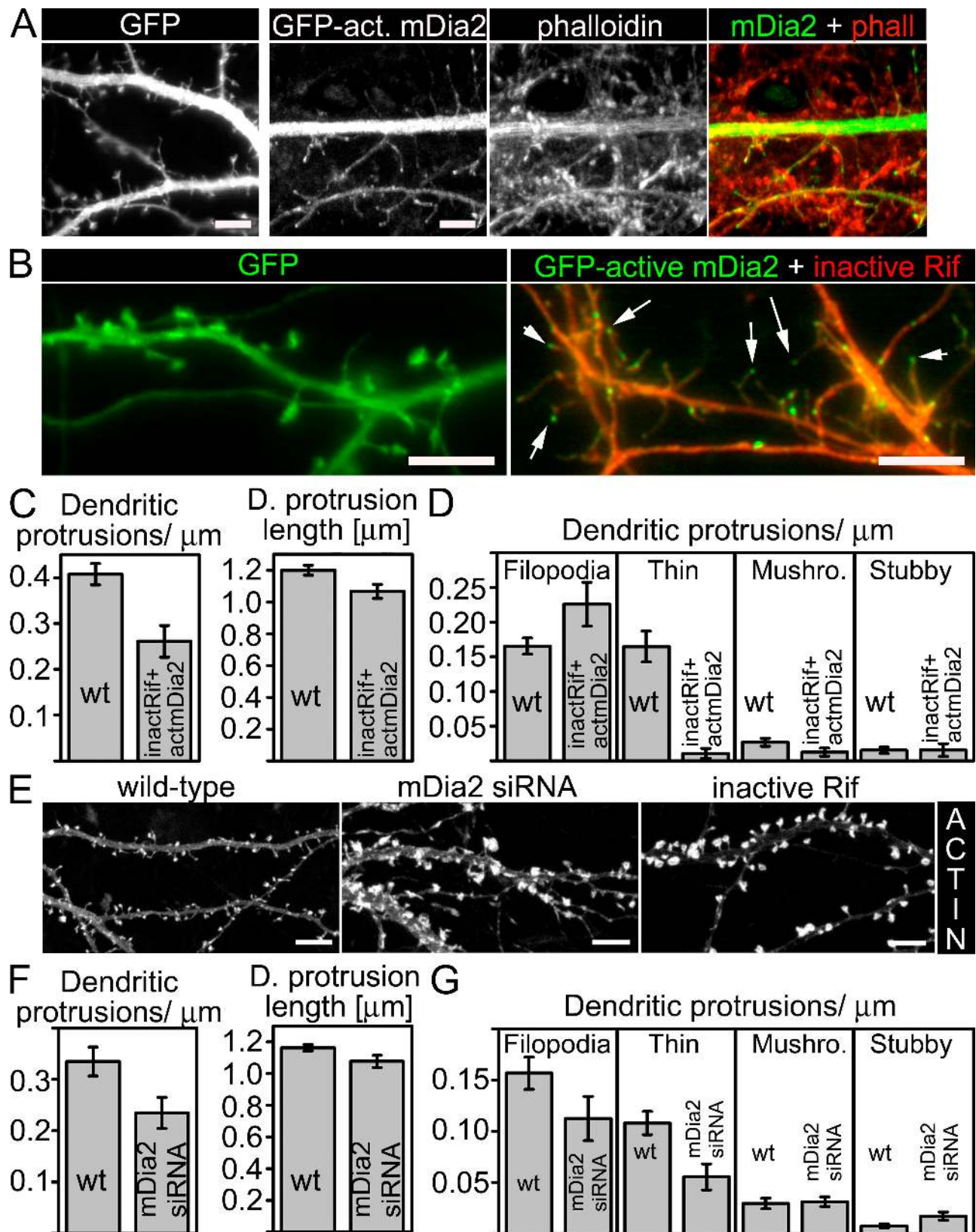
Figure 3. **Role of mDia2 in spinogenesis.** (A) Mouse hippocampal neurons were transfected with a plasmid expressing GFP (left) or a GFP fusion of active mDia2 construct at DIV 11, then fixed and stained with phalloidin at DIV 12. Active mDia2 localized to the filopodia tips, and its expression induced filopodia and spine head loss. (B) Mouse hippocampal neurons were transfected with GFP (left) or GFP-active mDia2 (green) and inactive Rif-myc (red) constructs at DIV 12; the cells were fixed and stained with anti-myc antibodies at DIV 13. Expression of active mDia2 overcomes the effect of inactive Rif. Arrows indicate the GFP-mDia2 tip localization. (C) Quantitative analysis of neurons expressing inactive Rif and active mDia2 (inactRif + actmDia2) showed significant reduction in dendritic protrusion density and length as compared with wild-type (wt) cells. Numerical data and p-values are presented in

Table IV. **Spine density and length quantification**

Description	n (neurons); DIV	n (spines)	Spine density (mean ± SEM)	P-value	Spine length (mean ± SEM)	P-value
			μm^{-1}		μm	
GFP control	16; 12	749	0.35 ± 0.022		1.22 ± 0.027	
Cdc42 GDP	15; 12	431	0.27 ± 0.027	**0.016**	1.07 ± 0.067	**0.004**
Cdc42 GTP	19; 12	648	0.28 ± 0.022	0.690[a]	0.95 ± 0.027	0.027[a]
				0.020		**<0.001**
GFP control	26; 12–13	1,296	0.27 ± 0.023	0.199	1.16 ± 0.018	
Inactive Rif	29; 12–13	994	0.24 ± 0.013		1.10 ± 0.019	**0.024**
GFP control	14; 12	749	0.35 ± 0.030		1.10 ± 0.025	0.824
Active Rif	18; 12	536	0.26 ± 0.018	**0.003**	1.11 ± 0.033	
GFP control	13; 12	697	0.37 ± 0.031		1.17 ± 0.026	0.292
Inactive Rif + WA	18; 12	334	0.25 ± 0.023	**0.005**	1.22 ± 0.046	
GFP control	19; 12–13	995	0.35 ± 0.028		1.16 ± 0.021	
mDia2 siRNA	12; 12–13	385	0.23 ± 0.030	**0.046**	1.08 ± 0.038	**0.027**
GFP control	12; 12 and 14	598	0.41 ± 0.023		1.20 ± 0.031	
Inactive Rif + active mDia2	12; 12 and 14	311	0.26 ± 0.035	**0.003**	1.07 ± 0.044	**0.012**
GFP control	37; 11–13	1,599	0.24 ± 0.018		1.19 ± 0.016	
p34 siRNA	28; 11–13	650	0.17 ± 0.015	**0.003**	1.40 ± 0.030	**<0.001**
W	14; 12	606	0.29 ± 0.025		1.29 ± 0.027	0.444
WA	15; 12	300	0.16 ± 0.011	**<0.001**	1.33 ± 0.047	
GFP control	22; 12–13	1,156	0.28 ± 0.026	0.070	1.15 ± 0.019	
cof1 siRNA	23; 12–13	982	0.23 ± 0.012		1.38 ± 0.025	**<0.001**
GFP control	17; 12	890	0.29 ± 0.032		1.17 ± 0.021	
cof1 siRNA	18; 12	702	0.21 ± 0.011	**0.047**	1.37 ± 0.029	**<0.001**
cof1 siRNA + cof1 rescue	20; 12	857	0.26 ± 0.019	0.577	1.45 ± 0.024	**<0.001**
				0.295[b]		0.117[b]

Statistically significant values (P < 0.050) are shown in bold.

[a]P-value for cdc42GDP:cdc42GTP.

[b]P-value for cof1 siRNA:cof1 siRNA + cof1 rescue.

effector mDia2 negatively regulate the formation of spine heads. Inactivation of Rif or mDia2 induced reduction in dendritic protrusion length, which suggests a positive role in protrusion elongation. However, it is important to note that activation of Rif or mDia2 could not induce an increase in the mean length of dendritic protrusions.

Polymerization of actin filaments in spine heads

We next examined the sites and mechanisms of actin polymerization in spine heads. Visualization of free actin filament barbed ends with fluorescently labeled actin monomers revealed that polymerization-competent barbed ends are not homogenously distributed throughout the spine head but are localized either as a "line" or dots at the spine head surface (Fig. 4, A–C). Barbed ends were also occasionally found from the roots of spine necks. However, the proportion of "mature" spines exhibiting barbed end localization to the roots was very small compared

with dendritic filopodia (Fig. 1, B and C; and Fig. 4, C and D), which suggests that root polymerization occurs mainly at early stages of spinogenesis. FRAP analysis yielded similar results, demonstrating that actin polymerization occurs as a line or dots on the spine head surface (Fig. 4 E). In the example presented in Fig. 4, actin monomers first incorporated into the "corners" of the spine head, followed by a rapid accumulation of actin to form a line at the spine surface (Fig. 4 E).

The exact role of the Arp2/3 complex in spine morphology is unknown. Western blot analysis revealed expression of Arp2/3 at all ages of hippocampal cultures analyzed (Fig. S4 A). Consistent with previous observations (Soderling et al., 2007; Wegner et al., 2008), endogenous Arp2/3 localized to the spine heads (Fig. S4 B). To examine the function of Arp2/3 in spine morphogenesis, we silenced the expression of the Arp2/3 complex p34 subunit by RNAi. The efficacy of the human homologous siRNA sequence was previously determined in U2OS cells (Hotulainen and Lappalainen, 2006). In neurons,

Table IV. (D) Dendritic protrusion morphology analysis of inactive Rif and active mDia2-expressing neurons revealed an increase in the number of filopodia and a significant decrease in the number of thin spines. Numerical data and p-values are presented in Tables I and II. (E) Mouse hippocampal neurons were transfected with GFP-actin, GFP-actin + mDia2 siRNA, or GFP-actin + inactive Rif constructs at DIV 12; the cells were fixed and stained with anti-mDia2 antibodies (Fig. S3) or anti-myc antibodies (not depicted) at DIV 13. Transfection of cells with mDia2 siRNA oligonucleotides resulted in dendritic protrusion morphology defects similar to those from expression of inactive Rif (shortened spine necks and larger spine heads). (F) Quantitative analysis of mDia2 siRNA-treated neurons showed a significant reduction in dendritic protrusion density and dendritic protrusion length as compared with wild type (wt). Numerical data and p-values are presented in Table IV. (G) Dendritic protrusion morphology analysis of mDia2 siRNA-treated neurons revealed a decrease in the number of filopodia and thin spines, and a significant increase in the number of stubby spines. Numerical data and p-values are presented in Tables I and II. Graphs represent mean ± SEM. Bars, 5 μm.

Figure 4. **Identification of the sites of actin filament polymerization in spine heads.** (A–C) The free actin filament barbed ends in mouse hippocampal neurons (DIV 12) were visualized with fluorescently labeled actin monomers (middle panels, barbed ends are indicated with arrowheads). F-actin was stained with fluorescently labeled phalloidin (left panels). Right panels show merged pictures. Barbed ends localized either as dots (A and C) or a "line" (B) at the spine head surface or to the root of the neck (C). (D) The number of sites (percentage of total spines analyzed) of barbed ends in different locations (tip of spine head [head tip] or tip of spine head + root of the neck [h. tip + n. root]) were counted from 128 spines from four independent experiments (DIV 12–16). The graph represents mean ± SEM. (E) Mouse hippocampal neurons were transfected with GFP-actin at DIV 20, and the FRAP assay was performed at DIV 21. GFP-actin was bleached from the spine head, and recovery of the GFP-actin fluorescence was followed by time-lapse imaging. The fluorescence of GFP-actin recovers mainly from the spine head tip. First sites of recovery are indicated with arrowheads. Bars, 1 µm.
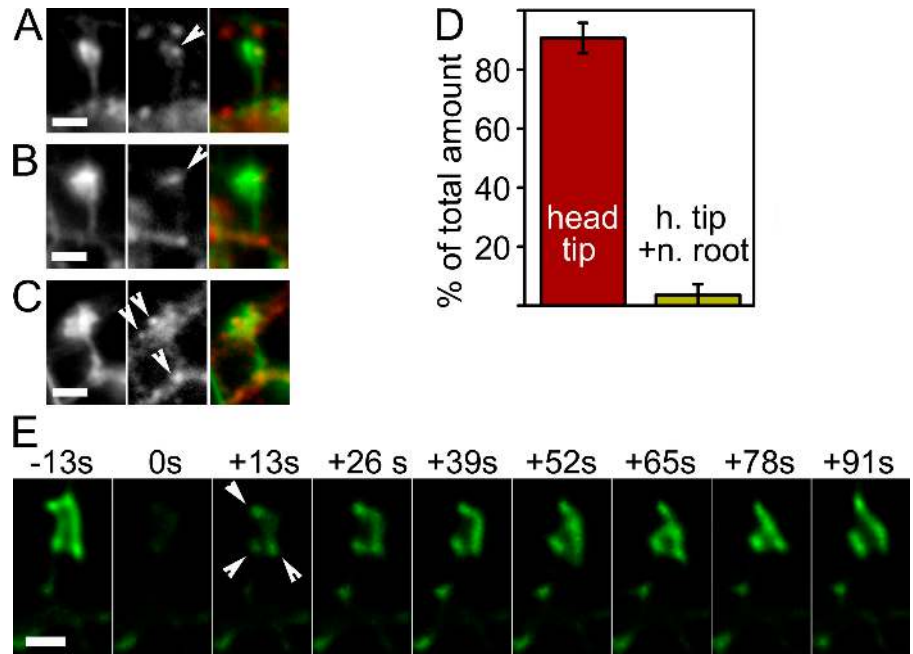
the silencing efficacy of p34 siRNA was determined similarly to the procedure for mDia2 siRNA. p34 antibody staining intensity in soma of GFP-expressing neurons was reduced by 52% compared with nontransfected neurons (Fig. S4, C and D). Decreased p34 expression resulted in a significantly lower density of dendritic protrusions with increased length (Fig. 5, A and B). Morphological analysis revealed an increase in the number of filopodia and a decrease in the number of thin, mushroom, and stubby spines (Fig. 5 C). The remaining dendritic filopodia exhibited relatively normal elongation dynamics, as visualized by time-lapse confocal stack imaging (Video 7 [wild-type] and Video 8 [p34 siRNA]), which suggests that Arp2/3 is not necessary for elongation of dendritic filopodia.

Similar spine/filopodia morphology was also achieved by disrupting the Arp2/3 localization through expression of the Scar1-WA fragment in DIV 12 hippocampal neurons, which demonstrates that the observed p34 knockdown phenotype was specific for depletion of the Arp2/3 complex (Fig. S4, E–G). Scar1-WA–expressing cells had a decreased number of thin, mushroom, and stubby spines, similar to p34 siRNA-treated cells (Fig. 5, A and C; and Fig. S4, E and G). Control cells expressing only the Scar1-W fragment, which binds actin monomers but does not interact with Arp2/3, did not display a decrease in dendritic protrusion density or changes in the distribution to different morphology classes (Fig. S4, E–G). However, Scar1-W–expressing cells showed longer dendritic protrusions as compared with cells expressing only GFP (Fig. 5, A and B; and Fig. S4, E and F). Together, these data suggest a central role for Arp2/3 in expansion of dendritic spine heads from the tip of filopodia-like spine precursors.

Coordination of Arp2/3- and mDia2-promoted actin filament polymerization

As Rif appeared to have a negative influence on the spine head formation and a positive influence on the dendritic protrusion elongation (whereas Arp2/3 had the opposite effects), we tested whether they antagonize each other in hippocampal neurons, as suggested previously for HeLa cells (Beli et al., 2008). Inhibition of Arp2/3 in cells expressing inactive Rif reduced the number of mushroom and stubby spines compared with cells expressing inactive Rif alone. Thus, the increased formation of stubby and mushroom spines upon inhibition of Rif is dependent on the Arp2/3 complex (Fig. 5, D–F). These data suggest interplay between Rif and Arp2/3 in the formation of dendritic spines but do not provide direct evidence for a Rif-mediated inhibition of Arp2/3 during spine morphogenesis. Furthermore, it is important to note that simultaneous inhibition of Arp2/3 and Rif did not result in a complete loss of dendritic protrusions, suggesting that other actin filament nucleation/polymerization pathways also contribute to spine morphogenesis.

Depolymerization of actin filaments

Not only is the polymerization of actin filaments required for rapid actin treadmilling, but the rapid disassembly of the filaments by ADF/cofilins is required as well (Bamburg, 1999). We performed initial siRNA and localization studies for both ADF and cofilin-1; however, because of similar results for these two isoforms (unpublished data), we focus here on cofilin-1. Western blot analysis revealed cofilin-1 expression in hippocampal neurons throughout spine development (Fig. S5 A). In accordance with previous data (Racz and Weinberg, 2006), endogenous cofilin-1 localized to the spine heads; however, high cofilin-1 levels were also found in the dendritic shaft (Fig. S5 B). Next, we used RNAi to examine the function of cofilin-1 in spine development. The efficacy of siRNA oligonucleotides was tested previously (Hotulainen et al., 2005). In neurons, the silencing efficacy of cofilin-1 siRNA was determined similarly to the procedure used for mDia2 siRNA. Cofilin-1 antibody staining intensity in soma of GFP-expressing neurons was reduced by 71% compared with nontransfected neurons (Fig. S5, C and D). Neurons with reduced cofilin-1 expression exhibited
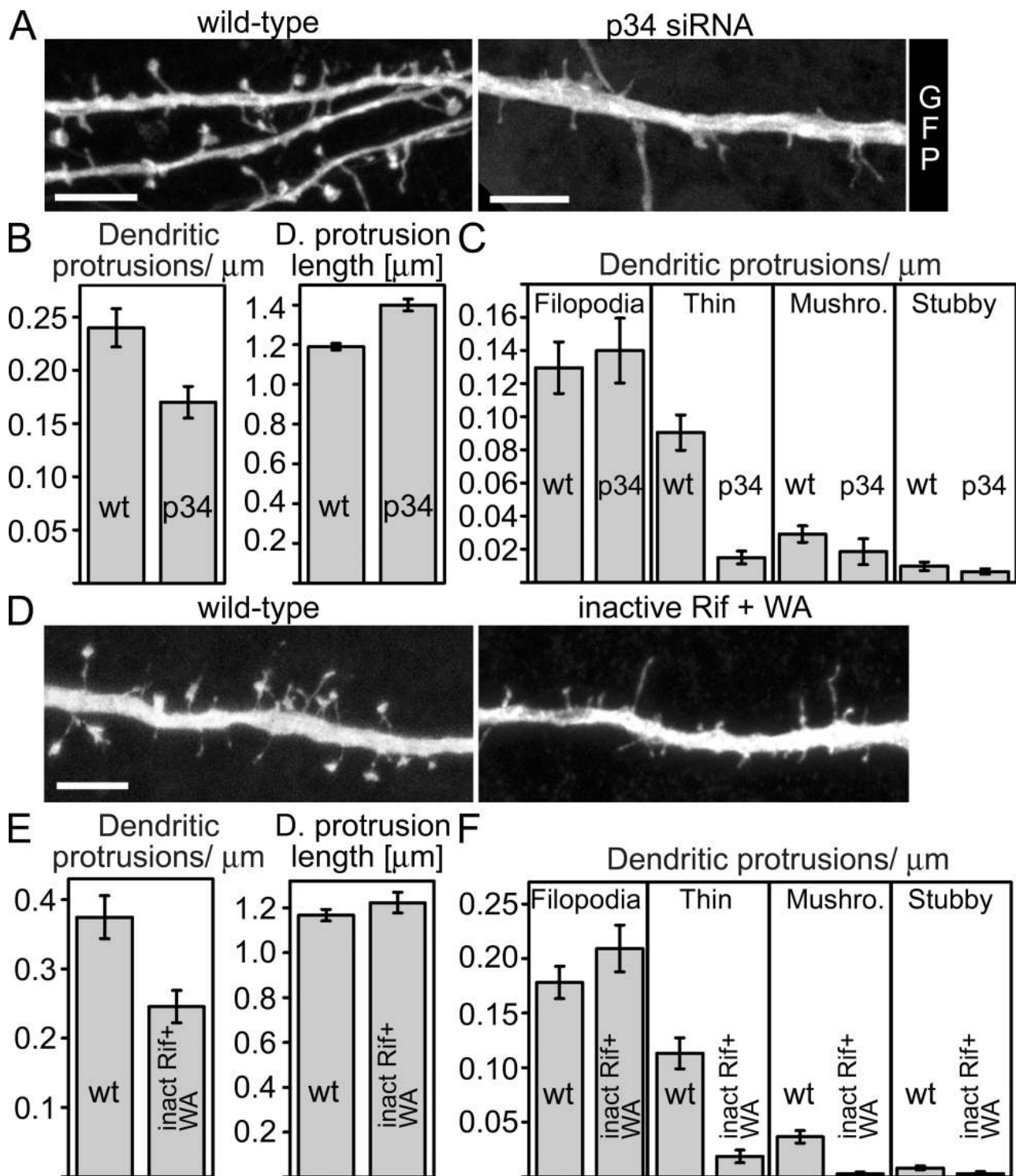
Figure 5. **Arp2/3 is necessary for spine head formation.** (A) Mouse hippocampal neurons were transfected with GFP or GFP + p34 siRNA at DIV 10. At DIV 11, the cells were fixed and stained with anti-p34 antibodies (see Fig. S4). Reduced p34 levels resulted in a loss of spine heads. Bars, 5 μm. (B) Dendritic protrusion density and length of p34 siRNA-transfected neurons was analyzed with NeuronIQ software (Cheng et al., 2007). Dendritic protrusion density was decreased and dendritic protrusion length increased in p34 siRNA-transfected cells compared with wild-type cells. See Tables I and II for numerical data. (C) Dendritic protrusion morphology analysis revealed a clear reduction of thin, mushroom, and stubby spines. See Tables I and II for numerical data. (D) Mouse hippocampal neurons were transfected with GFP (wt) or inactive Rif + Scar1-WA (inact Rif + WA) constructs at DIV 10. At DIV 11, cells were fixed and stained with anti-myc antibodies. Inhibition of Arp2/3 and Rif induced spine head loss. Bars, 5 μm. (E) Dendritic protrusion density was reduced, whereas mean dendritic protrusion length was not affected in cells expressing inactive Rif and Scar1-WA. See Table IV for numerical data. (F) Morphology analysis revealed a significant reduction in thin, mushroom, and stubby spines in cells expressing inactive Rif and Scar1-WA. See Tables I and II for numerical data. Graphs represent mean ± SEM.
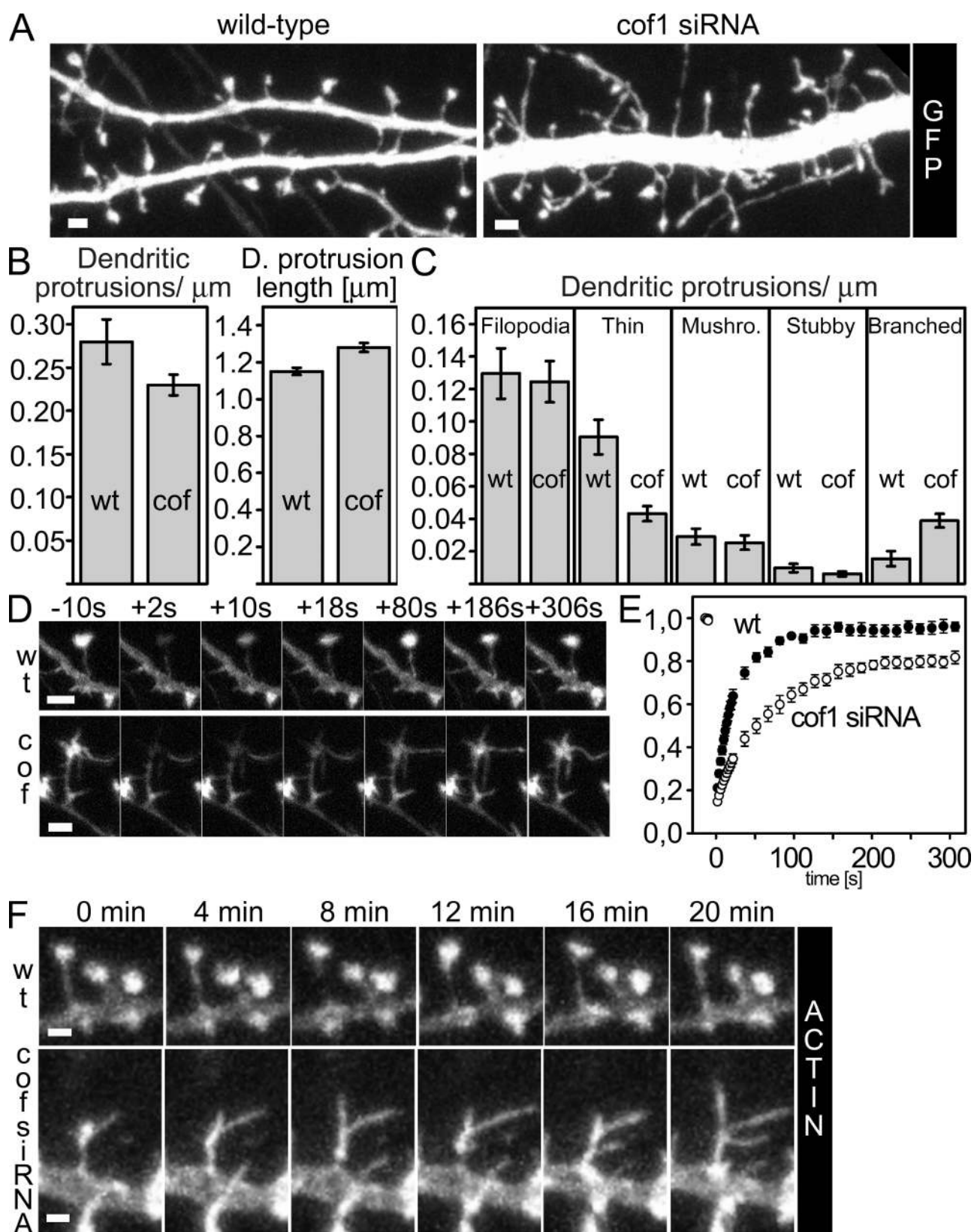
Figure 6. **Cofilin-1 is necessary for proper spine morphology and actin turnover.** (A) Mouse hippocampal neurons were transfected with GFP in the presence or absence of cofilin-1 siRNA oligonucleotides at DIV 11. On DIV 12, the cells were fixed and stained with anti–cofilin-1 antibodies (see Fig. S5). Reduction in cofilin-1 protein levels resulted in abnormal spine morphology (longer necks, branched spine heads). (B) Dendritic protrusions of wild-type and cofilin-1 siRNA-transfected cells were analyzed with NeuronIQ software (Cheng et al., 2007). Dendritic protrusion density was reduced and dendritic protrusion length was increased in cofilin-1 siRNA-transfected cells as compared with wild-type cells. Numerical data are presented in Table IV. (C) Morphology analysis revealed a decrease in the number of thin spines. Numerical data are presented in Tables I and II. Moreover, the density of branched

longer dendritic protrusions (Fig. 6, A and B). The most obvious defects in cofilin-1 knockdown cells were an increased branching of spines and a decreased number of thin spines (Fig. 6, A and C).

Because the depletion of cofilin-1 reduces the rate of actin filament turnover in fibroblasts (Hotulainen et al., 2005), we examined actin filament treadmilling rates in cofilin-1 knockdown neurons by FRAP. As described previously (Star et al., 2002), actin filament turnover in spine heads was extremely fast, with ~90% of GFP-actin fluorescence recovering within 2 min (Fig. 6, D and E). In contrast, actin filaments in spines of cells transfected with cofilin-1 siRNA oligonucleotides recovered more slowly, achieving ~80% recovery in ~4 min (Fig. 6, D and E). The obtained first order rate constant was threefold slower in cofilin-1 knockdown cells as compared with wild-type cells.

In other cell types tested, depletion of ADF/cofilins resulted in decreased dynamics of plasma membrane protrusions (e.g., Hotulainen et al., 2005). Thus, we expected that the dynamics of spines in cofilin-1 knockdown neurons would be diminished. To our surprise, the spines in cofilin-1 knockdown cells exhibited relatively rapid dynamics. However, small protrusions that rapidly appeared and disappeared in the wild-type spine heads grew for a longer period of time in cofilin-1 knockdown cells, resulting in the formation of spine heads with many filopodia-like branches (Fig. 6 F, Video 7 [wild-type], and Video 9 [cofilin-1 siRNA]).

The cofilin-1 knockdown phenotype could be rescued by cotransfection of the cells with an siRNA-resistant cofilin-1 construct (silent mutations introduced to the target sequence of siRNA oligonucleotides; see Hotulainen et al., 2005), confirming that the described cofilin-1 knockdown phenotypes indeed resulted from diminished cofilin-1 expression (Fig. S5, C–G).

Defects in the actin cytoskeleton and spine morphology affect the activity of neurons

We next examined whether depletion of cofilin-1, Arp2/3, and the Rif–mDia2 pathway results in defects in synapse number or activity. Visualization of synapses using the presynaptic marker vesicular glutamate transporter 1 (V-GLUT-1) revealed a slight decrease in the number of presynaptic contacts in Scar1-WA–expressing (Arp2/3 depletion) cells, whereas cells transfected with cofilin-1 siRNA or inactive Rif construct displayed a similar amount of synapses compared with control cells (Fig. 7, A and B).

We further explored the functionality of the manipulated neurons by recording the miniature excitatory postsynaptic currents (mEPSCs). The frequency of mEPSCs was strongly dependent on neuron age (DIV). In nontransfected cells and in the control cells transfected with GFP, the average median inter-event intervals in DIV 12, 13, and 14 cultures were 1,034 ± 181 ms ($n = 17$), 431 ± 95 ms ($n = 18$), and 237 ± 40 ms ($n = 8$), respectively. The amplitude of the mEPSCs was changed only slightly, with values of 10.9 ± 0.7 pA for DIV 12, 11.9 ± 0.7 pA for DIV 13, and 12.8 ± 1.6 pA for DIV 14.

Recordings of cells transfected with GFP with p34 siRNA (Arp2/3 depletion), cofilin-1 siRNA, or the inactive Rif construct from the same experimental day revealed that all three manipulations of the actin cytoskeleton increased the inter-event intervals, but there was no significant effect on event amplitude (Fig. 7, C and D). The mean relative effects (see Materials and methods) on the inter-event interval were 204 ± 52% in Arp2/3-depleted cells and 201 ± 49% in cells expressing inactive Rif (Fig. 7 E). Corresponding values for event amplitudes were 93 ± 5% and 95 ± 5%, respectively (Fig. 7 E). No significant changes were observed in cofilin-1 siRNA-transfected neurons on either inter-event interval (141 ± 30%) or event amplitudes 99 ± 8% (Fig. 7 E).

Discussion

Our data revealed that coordinated Arp2/3- and mDia2 formin-induced actin filament nucleation/polymerization, together with ADF/cofilin-induced actin filament disassembly, is critical to development and morphogenesis of dendritic spines. A working model for the mechanisms of actin filament assembly and disassembly during dendritic spine morphogenesis is shown in Fig. 8. In future studies, it will be important to complement this model by determining the precise roles and regulation of various actin-binding proteins during the development of dendritic spines.

Actin filament polymerization in filopodia-like precursors of dendritic spines occurs at the filopodia tips and roots

Live-cell microscopy analyses revealed that in "classical" filopodia, actin filament assembly occurs at the tip (for reviews see Gupton and Gertler, 2007; Mattila and Lappalainen, 2008). The surprising discovery of polymerization-competent barbed ends at both roots and tips in dendritic filopodia suggests that the shaft of dendritic filopodia (and perhaps also in mature spines) consists of an antiparallel organization of actin filaments (Fig. 8). Thus, although dendritic filopodia morphologically resemble canonical filopodia, their actin filament organization is distinct. In addition to an antiparallel filament bundle, dendritic filopodia and spine necks may also contain other types of F-actin structures that are not found in "classical" filopodia.

---

spines was increased from 0.015 to 0.039 spines per micrometer (P < 0.001) as compared with wild-type cells. Graphs represent mean ± SEM. (D) The rate of actin turnover was analyzed from wild-type and cofilin-1 siRNA-transfected cells by FRAP. Mouse cortical neurons were transfected with GFP-actin (wt) or with GFP-actin with cofilin-1 siRNA (cof) at DIV 11, and the FRAP analysis was performed at DIV 12. The frames before (−10 s) and after bleach (from +2 to +306 s) are shown. In the spines of wild-type neurons, the fluorescence of GFP-actin recovery was nearly complete at 80 s; in cofilin-1 siRNA neurons, complete recovery was not achieved within 306 s. (E) The averaged recovery curves from nine wild-type and seven cofilin-1 siRNA cells revealed a diminished rate of actin turnover in cofilin-1 siRNA-transfected cells. Error bars represent SEMs. (F) Dynamics of spines of wild-type and cofilin-1 siRNA-transfected cells were followed by time-lapse stack confocal scan microscopy. Mouse hippocampal neurons at DIV 11 (wild-type) or DIV 10 (cofilin-1 siRNA) were transfected with GFP-actin without (wt; Video 7) or with cofilin-1 siRNA oligonucleotides (cofsiRNA; Video 9), and the time-lapse videos were acquired on the day after the transfection. Note the slow removal of the filopodia-like protrusions from the spine head in the cofilin-1–depleted cell. Bars, 1 µm.
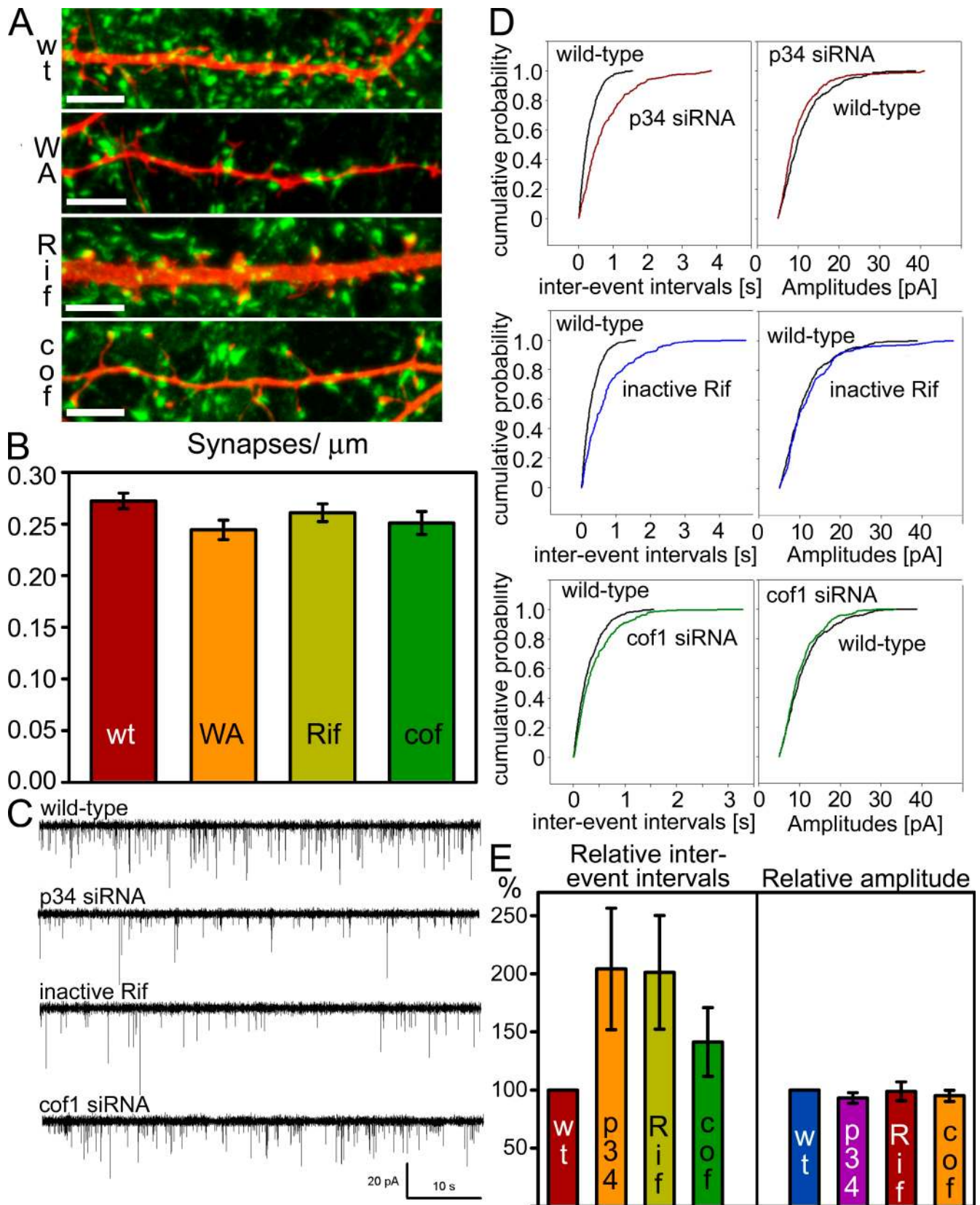
Figure 7. **Manipulation of the actin cytoskeleton affects the number of synapses and frequency of mEPSCs.** (A) Mouse hippocampal neurons were transfected with GFP + control siRNA oligonucleotides (wt), with a Scar1-WA construct (inhibits Arp2/3; WA), with an inactive Rif construct (Rif), or with GFP + cofilin-1 siRNA (cof) at DIV 11. At DIV 12, the cells were fixed and stained with anti–V-GLUT-1 antibodies (green) to label the presynaptic part of synapses. In addition, the cells expressing myc-tagged constructs, WA and Rif, were stained with anti-myc antibodies (red, as in GFP staining). Bars, 5 µm. (B) The number of synapses was counted with Imaris software from at least 10 cells from each group. The WA expression reduced the number of synapses from
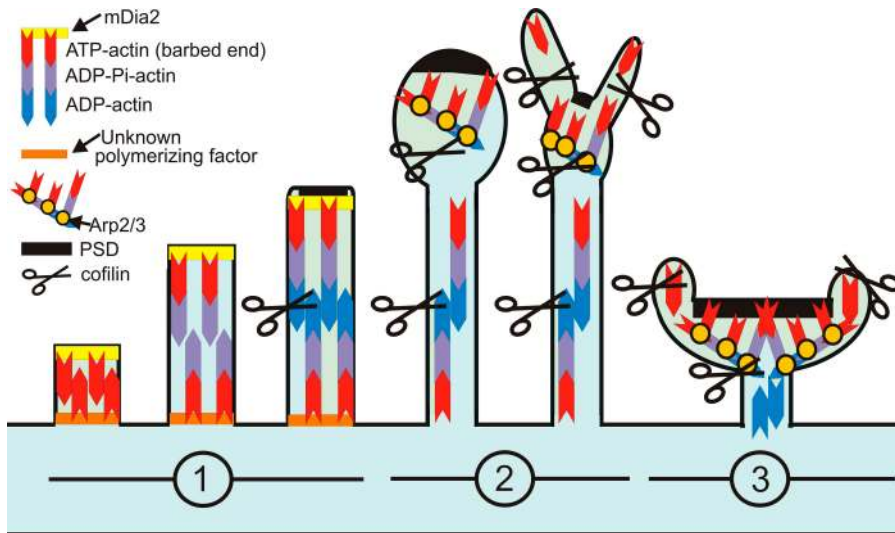
Figure 8. **A working model for the mechanisms of actin dynamics during dendritic spine development.** (1) Spine development starts with the initiation of the dendritic filopodium and its elongation. At this stage, the filopodia are highly dynamic, undergoing continuous elongation and shrinking. We propose that mDia2 promotes actin filament polymerization in the filopodium tip. The factors driving actin filament polymerization in the roots of filopodia remains to be identified. (2) The spine head begins to form. We propose that the mechanism of actin assembly is gradually changed from an mDia2-mediated polymerization of unbranched actin filaments to an Arp2/3-nucleated branched actin filament network, leading to enlargement of the spine head. The spine heads are highly dynamic, continuously changing their shape, and long protrusions from the spine heads are frequently seen. We propose that the function of ADF/cofilins, in addition to replenishing the cytoplasmic actin monomer pool in neurons, is to control the proper length of actin filaments and thus to prevent formation of abnormal protrusions from spine heads. Future studies will be required to reveal the exact spine locations where ADF/cofilins are active. (3) Mature spines are still dynamic but maintain their overall morphology. Dynamics occur as small protrusions on the surface of the spine head (morphing).

The most thoroughly studied pathways of filopodia formation in other cell types involve the small GTPases Cdc42 and Rif (Pellegrin and Mellor, 2005; Ridley, 2006). In agreement with previous results (Irie and Yamaguchi, 2002; Wegner et al., 2008), we found no involvement of Cdc42 in dendritic filopodia formation. However, we found that Rif and its downstream effector, mDia2 formin, play an important role in regulating dendritic filopodia formation. It is important to note that mammals have 15 formins, and it is thus possible that other formins also contribute to actin filament polymerization in dendritic spines. Moreover, it will be important to identify the nucleation factors that promote actin filament polymerization at the roots of dendritic filopodia.

Actin filament–nucleating Arp2/3 complex is important in spine head expansion from dendritic filopodia

Our analysis revealed that during expansion of spine heads and in the mature spine heads, rapid actin filament assembly is concentrated to small foci or as lines at the spine surface. These observations are in good agreement with previous studies that revealed a pool of highly dynamic actin filaments in the surface of spine heads (Honkura et al., 2008). Importantly, our analysis revealed that inactivation of the Arp2/3 complex leads to defects in the formation of bulbous spine heads from dendritic filopodia. These results expand previous findings showing that reduced Arp2/3 levels lead to a significant decrease in the number of dendritic protrusions (Wegner et al., 2008). Our data are also in good agreement with results from previous studies demonstrating that depletion/inactivation of known Arp2/3 complex regulators can lead to decreased dendritic protrusion density and spine morphogenesis defects (Grove et al., 2004; Kim et al., 2006; Proepper et al., 2007; Soderling et al., 2007). From these data, we propose that at a certain point during spine development, the actin assembly mechanism is gradually switched from mDia2, which promotes the formation of unbranched actin filament bundles, to the Arp2/3 complex, which induces formation of the branched actin filament network in the dendritic protrusion tip. This shift leads to the expansion of the spine head (Fig. 8). In support to this model, a recent study suggested that in HeLa cells, a complex with WAVE and Arp2/3 inhibits mDia2-induced filopodia formation and subsequently promotes membrane ruffling (Beli et al., 2008). However, whether Arp2/3 and mDia2 regulate each other during spine morphogenesis remains to be clarified.

Cofilin-1–induced actin filament disassembly is important to maintain spine morphology

Our data also revealed that actin filament disassembly by ADF/cofilin family proteins plays an important role in shaping the spine heads. In neurons with decreased amounts of cofilin-1,

0.27 to 0.24 per micrometer; P = 0.023. Rif expression or cofilin-1 siRNA transfections caused only a slight reduction to 0.26 per micrometer (P = 0.326) or 0.25 per micrometer (P = 0.122), respectively. The graph indicates SEMs. (C) Functional synapses were analyzed by measuring mEPSCs. Mouse hippocampal neurons were transfected with GFP alone (wild-type) or with GFP with p34 siRNA, with an inactive Rif construct, or with cofilin-1 siRNA. siRNA was transfected at DIV 11, and plasmids were transfected at DIV 13. Shown are representative recordings of spontaneous miniature glutamatergic postsynaptic currents of the neurons at DIV 14. (D) The cumulative probability plots from the recordings presented in C show an increased appearance of longer inter-event intervals for transfected cells but no obvious changes in the event amplitudes. (E) Diagram showing the overall effect of transfection with p34 or cofilin-1 siRNA or an inactive Rif construct on inter-event interval and event amplitude. Median inter-event intervals or amplitude of each manipulated cell have been divided by the wild-type values of the same experimental day (DIV 11–14). The mean time between events was twice as long in p34 siRNA (n = 9 experimental days, 27 cells, P = 0.009) or inactive Rif-transfected cells (n = 8 experimental days, 24 cells, P = 0.006) compared with control cells (43 cells). In cofilin-1 siRNA cells (n = 9 experimental days, 27 cells, P = 0.421), the corresponding increase was 1.4. The amplitude of currents did not change with any manipulation. The graphs indicate SEMs.

actin filament turnover rates in spines decreased by approximately threefold, and the spines typically contained abnormal filopodia-like protrusions or had aberrantly long spine necks. Previous studies showed that in LIMK1 −/− cells, which are expected to exhibit ADF/cofilin hyperactivity, spines are characterized by stubby (short thick neck, small head) morphology (Meng et al., 2002). Together, these data suggest that in addition to maintenance of rapid actin treadmilling, the second function of ADF/cofilins in these structures is promotion of strictly localized actin filament depolymerization/severing to ensure proper actin filament lengths in the spine neck and head, thus preventing the formation of abnormal plasma membrane protrusions in the spine head (Fig. 8). Cofilin is phosphorylated during long-term potentiation, and it has been suggested that cofilin phosphorylation induces an increase in spine head size (Fukazawa et al., 2003; Chen et al., 2007; Fedulov et al., 2007). However, according to our results, cofilin inactivation is not sufficient to induce mature mushroom spine morphology; thus, other changes in actin dynamics (e.g., activation of the Arp2/3 complex) are also required.

Actin dynamics perturbation through Rif, Arp2/3, or Cofilin-1 inactivation leads to defects in synaptic activity

Previous results showed that knockout of proteins acting on the actin cytoskeleton affect the number and activity of synapses. Furthermore, these alterations are associated with deficits in learning and memory in knockout mice (WAVE −/− [Soderling et al., 2003], Abi-2 −/− [Grove et al., 2004], and LIMK1 −/− [Meng et al., 2002]). Our analysis revealed significant changes in the density of thin, mushroom, and stubby spines in Arp2/3 disrupted neurons. This was associated with a reduction in the frequency of mEPSCs, which suggests that the number of functional synapses was diminished in the Arp2/3-inactivated cells. However, the total number of synapses in Arp2/3-inactivated cells was reduced by only ∼10% compared with control cells. This may be due to the fact that the dendritic shafts of cultured hippocampal neurons accommodate ∼50% of total number of synapses (Boyer et al., 1998). Taking into consideration the fact that changes in spine morphology may thus affect only a subpopulation of the dendritic synapses, relatively small effects in total synapse density are expected. In addition, compensatory redistribution of synapses at the dendritic shaft may occur in response to perturbation of the actin cytoskeleton. Very little is known about the requirement for maintenance and functionality of shaft synapses, and in particular their dependency on the intact cytoskeleton (Aoto et al., 2007).

Similarly, depletion of cofilin-1 led to a decrease in the number of thin, mushroom, and stubby spines, although the defects were smaller compared with inactivation of Arp2/3. Accordingly, cofilin-1 RNAi resulted in a modest reduction in the frequency of mEPSCs, which suggests a moderate reduction of the number of active excitatory synapses in these cells. Previous results have implicated cofilin in the morphological changes correlated with synaptic plasticity (Fukazawa et al., 2003; Zhou et al., 2004; Chen et al., 2007; Fedulov et al., 2007). The modest effects on both excitatory synaptic density and the frequency of mEPSCs in an experiment targeting cofilin-1 suggest that this protein is not involved in the steady-state maintenance of synaptic transmission. However, this does not contradict with the idea that cofilin-1 would be required in the mechanisms leading to synaptic plasticity.

Expression of inactive Rif resulted in a reduction in the frequency of mEPSCs similar to Arp2/3 depletion. Rif inactivation also decreased the number of thin spines but increased the number of mushroom and stubby spines. In contrast to Arp2/3 depletion, inactivation of Rif did not decrease the density of synapses. Thus, the Rif pathway appears to affect the frequency of mEPSCs by a different mechanism. A plausible possibility is that manipulation of Rif pathway affects the ratio of silent/active synapses. In the future, it will be important to examine in detail whether changes in Arp2/3, Rif, and cofilin-1 activity influence the composition and trafficking of glutamatergic synapses as well as their involvement in synaptic plasticity.

Materials and methods

Primary cultures and transient transfections
Cortex or hippocampus from mouse day 16 or 17 embryos was dissected and plated on coverslips coated with poly-D-L-ornithine at a density of 75,000 cells per coverslip (24-well plate) in Glia-enriched Neurobasal medium supplemented with B27 and L-glutamine (Invitrogen). Transient transfections of cortical or hippocampal neurons were performed with Lipofectamine 2000 (Invitrogen). A typical transfection mixture for one 24-well plate well contained 100 µl Neurobasal medium, 2 µl Lipofectamine, and 0.5–0.8 µg of DNA and/or 300 ng of siRNA oligonucleotides. Cells were incubated for 4 h with the transfection mixture before washing and the addition of growth medium.

Plasmid construction and siRNA oligonucleotides
pEGFP-N1 plasmid (GFP) was purchased from Clontech Laboratories, Inc. Human GFP–β-actin (Choidas et al., 1998) and mCherry–β-actin plasmids were gifts from M. Bähler (Westfalian Wilhelms-University, Münster, Germany). Myc-tagged GTPase-deficient, activated construct, Rif-QL, and a constitutively GDP-bound inactive mutant, Rif-TN construct (Ellis and Mellor, 2000) were gifts from H. Mellor (University of Bristol, Bristol, England, UK). EGFP-tagged, constitutively active-DRF3/mDia2 (human, N-terminal 263 residues deleted) was provided by K. Rottner and T. Stradal (Helmholtz Centre for Infection Research, Braunschweig, Germany). Myc-tagged Scar1-W and -WA fragments (Machesky and Insall, 1998) were gifts from L. Machesky (University of Birmingham, Birmingham, England, UK). pEGFP-Cdc42 plasmids (Vartiainen et al., 2000) were gifts from J. Peränen (Institute of Biotechnology, Helsinki, Finland). The myc-tagged cofilin-1 rescue construct has been described previously (Hotulainen et al., 2005). The siRNA oligonucleotide target sequences were mDia2, sequence 1: 5′-ATA-AGAGAGCAGTATTTCAAA-3′ (Yang et al., 2007); mDia2, sequence 2: 5′-AATGCTCAAACCTTCGGATTT-3′; p34: 5′-AAGGAACTTCAGGCA-CATGGA-3′; cofilin-1: 5′-AAGGAGGACCTGGTGTTCATC-3′ (Bertling et al., 2004), and control: 5′-TAGCGCTGATGGCCAGATTTT-3′.

Antibodies
Proteins were visualized by immunofluorescence staining as follows: myc-tagged constructs, mouse anti-c-Myc antibody (1:200; Sigma-Aldrich); p34, rabbit polyclonal anti-p34 antibody (1:50; Millipore); cofilin-1, rabbit polyclonal anti–cofilin-1 antibody (1:100; Vartiainen et al., 2002); V-GLUT-1, guinea pig polyclonal anti–V-GLUT-1 antibody (1:800; Millipore); and mDia2, rabbit anti-mDia2 antibodies (1:50). Secondary antibodies were conjugated to FITC/Alexa Fluor 488, rhodamine/Alexa Fluor 568, or Cy5 (Invitrogen). F-actin was visualized with Alexa Fluor 488–, 568–, or 594–phalloidin (1:100 or 1:400; Invitrogen). For Western blotting, antibodies were used in 10-fold dilutions. Total actin was detected by anti-actin AC-15 antibody (1:10,000; Sigma-Aldrich).

Barbed end assay, immunofluorescence staining, and analysis of siRNA-treated cells
The barbed end assay was performed as described previously (Symons and Mitchison, 1991; Gupton et al., 2007). Alexa Fluor 568 or Alexa

Fluor 488–labeled rabbit actin monomers were obtained from Invitrogen. After fixation, cells were stained either with Alexa Fluor 488–phalloidin or 594–phalloidin (Invitrogen), respectively. Immunofluorescence was performed as described previously (Vartiainen et al., 2000). The mDia2/p34/cofilin-1 expression levels were analyzed from GFP-expressing neurons with TINA software (Imaging Science and Biomedical Engineering Research Group, University of Manchester) and compared with the neighboring cells not expressing GFP. In siRNA-treated cultures, there were also cells that displayed faint antibody staining but a lack of GFP expression. These cells were most likely transfected with siRNA but not with GFP (these are especially clearly seen in Fig. S5, where anti–cofilin-1 antibody staining can be compared with the anti-myc background staining). Such cells with significantly reduced antibody staining were not found from cultures transfected with the GFP plasmid alone.

Preparation of samples for Western blotting
Cells for Western blotting were normally washed three times with cold PBS, scraped, and lysed with PBS containing 1% Triton X-100 and 0.3 mM PMSF. Total protein concentrations were measured using Bradford reagent (Sigma-Aldrich). For mDia2 blots, a special protocol from the laboratory of H. Higgs (Dartmouth Medical School, Hanover, NH) was used. Cells were lysed with lysis buffer (50 mM Hepes, pH 7.2, 4% SDS, 300 mM NaCl, 1 mM EDTA, proteinase inhibitor cocktail, and 5 mM DTT) and boiled. After boiling, N-ethyl maleimide was added to the samples for the end concentration of 30 mM. Finally, samples were mixed 1:1 in SDS-PAGE loading buffer (including 1,000 mM NaCl, 4 M urea, and 140 mM β-mercaptoethanol) and loaded onto an SDS-PAGE gel.

Microscope setups for images and videos
Fig. 1, A and B; Fig. 3, A and B; Fig. 4, A–C; Fig. S4, B and C; and Fig. S5, B and C. Images were acquired with a charge-coupled device camera (U-CMAD3; Olympus) on an epifluorescent microscope (AX70 Provis; Olympus). For the image acquirement, the AnalySIS software (Olympus) and UPlan-Fluor 20×/0.50 (air) or UPlan-Apochromat 100×/1.35 (oil) objectives (Olympus) were used.

Fig. S1 D and Videos 3, 5, and 6. These time-lapse images were acquired with an inverted microscope (IX-71; Olympus) equipped with a Polychrome IV monochromator (TILL Photonics, GmbH) with the appropriate filters, heated sample environment (37°C), and CO_2 control (Solent Scientific). A UPlanS-Apochromat 60× W/1.20 (water) objective (Olympus) with or without 1.6× magnification was used. The software used for the image acquisition was TILL Vision 4 (TILL Photonics). The EM charge-coupled device camera used for the study was Andor iXon DV885 (Andor). Normal growth medium (glia-enriched Neurobasal medium supplemented with B27 and L-glutamine (Invitrogen) was used as an imaging medium in all time-lapse video captures.

All other figures and videos. Most of the figures and time-lapse videos were acquired with two confocal microscopes: (1) TCS SP2 AOBS confocal microscope (Leica) equipped with Leica Confocal software (2.61.1537), cube and box heating (37°C), and a CO_2 control system (LIS). For GFP imaging, a 70-mW 488-nm line of an Argon laser and an HCX Plan-Apochromat 63×/1.4–0.6 (oil; for fixed samples) or HCX Plan-Apochromat 63×/1.2 W Corr/0.17 CS (water; for living cells) objective lenses (Leica) were used. (2) TCS SP5 (Leica) equipped with LAS AF 1.82. Lasers used were a 561 nm/20 mW diode-pumped solid-state and a 488-nm line of a 100 mW Argon; the objective used was an HCX Apochromat 63×/1.30 (glycerol) corr CS 21 lens (Leica). Acquired confocal stacks are presented in figures as Max projection (Easy 3D) created by Bitplane Imaris suite software (Bitplane AG).

Deconvolution of images and videos:
Figs. 4 D and S1, C and E; Videos 2 and 3; and all images for synapse counting. These time-lapse videos or 3D images were deconvoluted by AutoQuant AutoDeblur 2D or 3D Blind Deconvolution software (Media Cybernetics).

Analysis of FRAP data
The recovery of the GFP-actin intensity was measured using Leica Confocal Software. The intensity of the bleached area was normalized to a neighboring nonbleached dendritic area to diminish error caused by normal photobleaching during the monitoring period. Bleached areas used for measurements were outlined to contain only the spine head. The value before bleach was normalized to 1.0. From each analyzed cell, three different areas for a total of at least six bleached spine heads were analyzed. The values from different spine heads of each analyzed cell were averaged,

and the mean values were charted in a scatter plot. The recovery half-time ($t_{1/2}$) was determined from these plots, and the k_{obs} values (first-order rate constant) were calculated by using the equation $k_{obs} = 0.693/t_{1/2}$. The averaged "cell values" from different cells were further averaged and charted in scatter plot shown in Fig. 6 D.

Quantitative analysis of dendritic protrusion morphology
Dendritic protrusion density (including all protrusions with different morphologies) and length were measured by NeuronIQ software from Nyqvist-sampled confocal stacks taken with a 63× objective lens according to Cheng et al. (2007), except that 1-pixel-wide Gaussian filtering in Imaris 6.0 (Bitplane) was used instead of median filtering. The densities of dendritic protrusions with different morphologies were counted from same confocal stacks. Definitions for different morphologies used for counting were: filopodia, thin protrusions without a distinguishable head; thin spines, thin protrusions with a distinguishable head, typically long neck, and small head with a width <0.75 µm; mushroom spines, typically a short neck and large head with a width >0.75 µm; and stubby spines, no distinct neck. The head widths of thin and mushroom spines were measured with ImageJ.

Synapse counting
The synapses were detected by partial colocalization of anti–V-GLUT-1 (labels the presynaptic sites of synapses) antibody staining with the transfected cell GFP fluorescence or myc tag staining. The synapses from deconvoluted confocal image stacks were counted using the Bitplane Imaris suite software. A surface was rendered comprehending the GFP/myc volume, and the V-GLUT-1–positive spots that were close enough were counted using the spots near surface function in the ImarisXT module as synaptic terminals. The maximum distance between GFP/myc and presynaptic terminals was set to 0.68 µm. From each group, at least 10 cells from two independent experiments and three different areas from each cell were analyzed.

Patch clamp recordings
Miniature postsynaptic currents (mPSCs) were recorded from mouse hippocampal cultured neurons (DIV 12–14) in a whole-cell voltage-clamp configuration at room temperature. The composition of the extracellular solution was: 124 mM NaCl, 3 mM KCl, 2 mM $CaCl_2$, 1.1 mM NaH_2PO_4, 1.3 mM $MgSO_4$, 20 mM Hepes, and 10 mM D-glucose, pH 7.4. Neurons were in the extracellular solution maximally for 2 h. To eliminate synchronized action potential–induced spontaneous postsynaptic currents, all experiments were performed in the presence of 1 µM TTX. Glutamatergic mPSCs were isolated by extracellular application of 10 µM bicuculline methiodide. Patch pipettes were fabricated from borosilicate glass (GC-150F; Harvard Apparatus); and their resistance, when filled with intracellular solution containing 18 mM KCl, 111 mM potassium gluconate, 0.5 mM $CaCl_2$, 5 mM BAPTA, 2 mM Mg-ATP, 10 mM Hepes, 10 mM glucose, and 2 mM NaOH, at pH 7.3, ranged from 6 to 8 MΩ. Membrane potential was clamped at −60 mV. Only cells with access resistance that did not exceed 20 MΩ were accepted for analysis. Access- and cell membrane resistance were regularly checked by 10-mV hyperpolarizing voltage pulses 100 ms long, and recordings were terminated if any of these resistances changed by 10% or more.

Data acquisition and analysis
A patch-clamp amplifier (EPC 9; HEKA) was used for voltage clamp and data acquisition. Data were acquired at sampling rate of 2 kHz and then band-pass filtered (1 Hz–1 kHz). Synaptic events were detected and analyzed using Mini Analysis software (version 6; Synaptosoft Inc.). After automatic screening (amplitude threshold set to 5 pA), events were approved manually according to their onset and decay. Because glutamatergic synaptic activity strongly depends on the DIV, the effect of each transfection agent was assessed from recordings obtained the same day. Only recordings that contained at least 200 synaptic events were accepted for analysis. The inter-event interval and event amplitude for each individual cell were characterized by their median values. The mean of median inter-event intervals and event amplitudes for each experimental paradigm was normalized to corresponding mean control values for each experimental day.

Statistical methods
Statistical significances for dendritic protrusion length measurements were calculated using t tests when two populations were compared and by analysis of variance (ANOVA) and related post-hoc tests (Scheffe) if more than two populations were compared with each other. Statistical significances of dendritic protrusion densities were calculated using Mann-Whitney U test.

The number of analyzed subjects and p-values are specified in Tables I–IV. P-values for other measurements are specified in figure letters; depending on the number of subjects, either a *t* test or Mann-Whitney *U* test was used. The p-values for Fig. 7 E were counted from the raw data where daily differences have been adjusted by Bonferroni correction.

Online supplemental material
Fig. S1 demonstrates the short- and long-term morphological changes occurring during spinogenesis. Fig. S2 shows the effects of active and inactive Cdc42 expression on dendritic protrusion morphology. Figs. S3, S4, and S5 show the effects of different siRNA treatments on the expression levels of target proteins (S3: mDia2; S4: p34; S5: cofilin-1). In addition, Fig. S4 shows the effect of Arp2/3 inhibition by Scar1-WA fragment expression to dendritic protrusion morphology, and Fig. S5 demonstrates that the phenotype achieved by cofilin-1 siRNA treatment can be rescued by expression of an siRNA nonsensitive cofilin-1 construct. Video 1 shows dendritic protrusion dynamics in DIV 8, 14, and 21 hippocampal neurons visualized by GFP-actin. Video 2 is a deconvolution of the DIV 21 panel in Video 1. Videos 3 and 4 present actin dynamics and morphological changes of individual spines. Videos 5–9 show spine dynamics in hippocampal neurons transfected with GFP-actin only (Video 5: control video for Video 6; Video 7: control video for Videos 8 and 9) or GFP-actin in combination with mDia2 siRNA (Video 6), p34 siRNA (Video 8), or cofilin-1 siRNA (Video 9). Online supplemental material is available at http://www.jcb.org/cgi/content/full/jcb.200809046/DC1.

References

Aoto, J., P. Ting, B. Maghsoodi, N. Xu, M. Henkemeyer, and L. Chen. 2007. Postsynaptic EphrinB3 promotes shaft glutamatergic synapse formation. *J. Neurosci.* 27:7508–7519.

Bamburg, J.R. 1999. Proteins of the ADF/cofilin family: essential regulators of actin dynamics. *Annu. Rev. Cell Dev. Biol.* 15:185–230.

Beli, P., D. Mascheroni, D. Xu, and M. Innocenti. 2008. WAVE and Arp2/3 jointly inhibit filopodium formation by entering into a complex with mDia2. *Nat. Cell Biol.* 10:849–857.

Bertling, E., P. Hotulainen, P.K. Mattila, T. Matilainen, M. Salminen, and P. Lappalainen. 2004. Cyclase-associated protein 1 (CAP1) promotes cofilin-induced actin dynamics in mammalian nonmuscle cells. *Mol. Biol. Cell.* 15:2324–2334.

Block, J., T.E. Stradal, J. Hänisch, R. Geffers, S.A. Köstler, E. Urban, J.V. Small, K. Rottner, and J. Faix. 2008. Filopodia formation induced by active mDia2/Drf3. *J. Microsc.* 231:506–517.

Boyer, C., T. Schikorski, and C.F. Stevens. 1998. Comparison of hippocampal dendritic spines in culture and in brain. *J. Neurosci.* 18:5294–5300.

Calabrese, B., M.S. Wilson, and S. Halpain. 2006. Development and regulation of dendritic spine synapses. *Physiology (Bethesda).* 21:38–47.

Carlier, M.F., and D. Pantaloni. 2007. Control of actin assembly dynamics in cell motility. *J. Biol. Chem.* 282:23005–23009.

Chen, L.Y., C.S. Rex, M.S. Casale, C.M. Gall, and G. Lynch. 2007. Changes in synaptic morphology accompany actin signaling during LTP. *J. Neurosci.* 27:5363–5372.

Cheng, J., X. Zhou, E. Miller, R.M. Witt, J. Zhu, B.L. Sabatini, and S.T. Wong. 2007. A novel computational approach for automatic dendrite spines detection in two-photon laser scan microscopy. *J. Neurosci. Methods.* 165:122–134.

Choidas, A., A. Jungbluth, A. Sechi, J. Murphy, A. Ullrich, and G. Marriott. 1998. The suitability and application of a GFP-actin fusion protein for long-term imaging of the organization and dynamics of the cytoskeleton in mammalian cells. *Eur. J. Cell Biol.* 77:81–90.

Dent, E.W., A.V. Kwiatkowski, L.M. Mebane, U. Philippar, M. Barzik, D.A. Rubinson, S. Gupton, J.E. Van Veen, C. Furman, J. Zhang, et al. 2007. Filopodia are required for cortical neurite initiation. *Nat. Cell Biol.* 9:1347–1359.

Ellis, S., and H. Mellor. 2000. The novel Rho-family GTPase rif regulates coordinated actin-based membrane rearrangements. *Curr. Biol.* 10:1387–1390.

Ethell, I.M., and E.B. Pasquale. 2005. Molecular mechanisms of dendritic spine development and remodeling. *Prog. Neurobiol.* 75:161–205.

Faix, J., and K. Rottner. 2006. The making of filopodia. *Curr. Opin. Cell Biol.* 18:18–25.

Fedulov, V., C.S. Rex, D.A. Simmons, L. Palmer, C.M. Gall, and G. Lynch. 2007. Evidence that long-term potentiation occurs within individual hippocampal synapses during learning. *J. Neurosci.* 27:8031–8039.

Fifková, E., and R.J. Delay. 1982. Cytoplasmic actin in neuronal processes as a possible mediator of synaptic plasticity. *J. Cell Biol.* 95:345–350.

Fukazawa, Y., Y. Saitoh, F. Ozawa, Y. Ohta, K. Mizuno, and K. Inokuchi. 2003. Hippocampal LTP is accompanied by enhanced F-actin content within the dendritic spine that is essential for late LTP maintenance in vivo. *Neuron.* 38:447–460.

Goode, B.L., and M.J. Eck. 2007. Mechanism and function of formins in the control of actin assembly. *Annu. Rev. Biochem.* 76:593–627.

Grove, M., G. Demyanenko, A. Echarri, P.A. Zipfel, M.E. Quiroz, R.M. Rodriguiz, M. Playford, S.A. Martensen, M.R. Robinson, W.C. Wetsel, et al. 2004. ABI2-deficient mice exhibit defective cell migration, aberrant dendritic spine morphogenesis, and deficits in learning and memory. *Mol. Cell. Biol.* 24:10905–10922.

Gupton, S.L., and F.B. Gertler. 2007. Filopodia: the fingers that do the walking. *Sci. STKE.* 2007:re5.

Gupton, S.L., K. Eisenmann, A.S. Alberts, and C.M. Waterman-Storer. 2007. mDia2 regulates actin and focal adhesion dynamics and organization in the lamella for efficient epithelial cell migration. *J. Cell Sci.* 120:3475–3487.

Hirokawa, N. 1989. The arrangement of actin filaments in the postsynaptic cytoplasm of the cerebellar cortex revealed by quick-freeze deep-etch electron microscopy. *Neurosci. Res.* 6:269–275.

Honkura, N., M. Matsuzaki, J. Noguchi, G.C. Ellis-Davies, and H. Kasai. 2008. The subspine organization of actin fibers regulates the structure and plasticity of dendritic spines. *Neuron.* 57:719–729.

Hotulainen, P., and P. Lappalainen. 2006. Stress fibers are generated by two distinct actin assembly mechanisms in motile cells. *J. Cell Biol.* 173:383–394.

Hotulainen, P., E. Paunola, M.K. Vartiainen, and P. Lappalainen. 2005. Actin-depolymerizing factor and cofilin-1 play overlapping roles in promoting rapid F-actin depolymerization in mammalian nonmuscle cells. *Mol. Biol. Cell.* 16:649–664.

Irie, F., and Y. Yamaguchi. 2002. EphB receptors regulate dendritic spine development via intersectin, Cdc42 and N-WASP. *Nat. Neurosci.* 5:1117–1118.

Kaksonen, M., C.P. Toret, and D.G. Drubin. 2006. Harnessing actin dynamics for clathrin-mediated endocytosis. *Nat. Rev. Mol. Cell Biol.* 7:404–414.

Kasai, H., M. Matsuzaki, J. Noguchi, N. Yasumatsu, and H. Nakahara. 2003. Structure-stability-function relationships of dendritic spines. *Trends Neurosci.* 26:360–368.

Kim, Y., J.Y. Sung, I. Ceglia, K.W. Lee, J.H. Ahn, J.M. Halford, A.M. Kim, S.P. Kwak, J.B. Park, S. Ho Ryu, et al. 2006. Phosphorylation of WAVE1 regulates actin polymerization and dendritic spine morphology. *Nature.* 442:814–817.

Kovar, D.R., E.S. Harris, R. Mahaffy, H.N. Higgs, and T.D. Pollard. 2006. Control of the assembly of ATP- and ADP-actin by formins and profilin. *Cell.* 124:423–435.

Landis, D.M., and T.S. Reese. 1983. Cytoplasmic organization in cerebellar dendritic spines. *J. Cell Biol.* 97:1169–1178.

Machesky, L.M., and R.H. Insall. 1998. Scar1 and the related Wiskott-Aldrich syndrome protein, WASP, regulate the actin cytoskeleton through the Arp2/3 complex. *Curr. Biol.* 8:1347–1356.

Mattila, P.K., and P. Lappalainen. 2008. Filopodia: molecular architecture and cellular functions. *Nat. Rev. Mol. Cell Biol.* 9:446–454.

Meng, Y., Y. Zhang, V. Tregoubov, C. Janus, L. Cruz, M. Jackson, W.Y. Lu, J.F. MacDonald, J.Y. Wang, D.L. Falls, and Z. Jia. 2002. Abnormal spine morphology and enhanced LTP in LIMK-1 knockout mice. *Neuron.* 35:121–133.

Meng, Y., H. Takahashi, J. Meng, Y. Zhang, G. Lu, S. Asrar, T. Nakamura, and Z. Jia. 2004. Regulation of ADF/cofilin phosphorylation and synaptic function by LIM-kinase. *Neuropharmacology.* 47:746–754.

Okamoto, K., T. Nagai, A. Miyawaki, and Y. Hayashi. 2004. Rapid and persistent modulation of actin dynamics regulates postsynaptic reorganization underlying bidirectional plasticity. *Nat. Neurosci.* 7:1104–1112.

Oray, S., A. Majewska, and M. Sur. 2006. Effects of synaptic activity on dendritic spine motility of developing cortical layer v pyramidal neurons. *Cereb. Cortex.* 16:730–741.

Pellegrin, S., and H. Mellor. 2005. The Rho family GTPase Rif induces filopodia through mDia2. *Curr. Biol.* 15:129–133.

Peng, J., B.J. Wallar, A. Flanders, P.J. Swiatek, and A.S. Alberts. 2003. Disruption of the Diaphanous-related formin Drf1 gene encoding mDia1 reveals a role for Drf3 as an effector for Cdc42. *Curr. Biol.* 13:534–545.

Pollard, T.D. 2007. Regulation of actin filament assembly by Arp2/3 complex and formins. *Annu. Rev. Biophys. Biomol. Struct.* 36:451–477.

Pollard, T.D., and G.G. Borisy. 2003. Cellular motility driven by assembly and disassembly of actin filaments. *Cell.* 112:453–465.

Proepper, C., S. Johannsen, S. Liebau, J. Dahl, B. Vaida, J. Bockmann, M.R. Kreutz, E.D. Gundelfinger, and T.M. Boeckers. 2007. Abelson interacting protein 1 (Abi-1) is essential for dendrite morphogenesis and synapse formation. *EMBO J.* 26:1397–1409.

Racz, B., and R.J. Weinberg. 2006. Spatial organization of cofilin in dendritic spines. *Neuroscience.* 138:447–456.

Ridley, A.J. 2006. Rho GTPases and actin dynamics in membrane protrusions and vesicle trafficking. *Trends Cell Biol.* 16:522–529.

Sacchetti, P., R. Carpentier, P. Ségard, C. Olivé-Cren, and P. Lefebvre. 2006. Multiple signaling pathways regulate the transcriptional activity of the orphan nuclear receptor NURR1. *Nucleic Acids Res.* 34:5515–5527.

Schirenbeck, A., T. Bretschneider, R. Arasada, M. Schleicher, and J. Faix. 2005. The Diaphanous-related formin dDia2 is required for the formation and maintenance of filopodia. *Nat. Cell Biol.* 7:619–625.

Sekino, Y., N. Kojima, and T. Shirao. 2007. Role of actin cytoskeleton in dendritic spine morphogenesis. *Neurochem. Int.* 51:92–104.

Soderling, S.H., L.K. Langeberg, J.A. Soderling, S.M. Davee, R. Simerly, J. Raber, and J.D. Scott. 2003. Loss of WAVE-1 causes sensorimotor retardation and reduced learning and memory in mice. *Proc Natl Acad Sci USA.* 100:1723–1728.

Soderling, S.H., E.S. Guire, S. Kaech, J. White, F. Zhang, K. Schutz, L.K. Langeberg, G. Banker, J. Raber, and J.D. Scott. 2007. A WAVE-1 and WRP signaling complex regulates spine density, synaptic plasticity, and memory. *J. Neurosci.* 27:355–365.

Star, E.N., D.J. Kwiatkowski, and V.N. Murthy. 2002. Rapid turnover of actin in dendritic spines and its regulation by activity. *Nat. Neurosci.* 5:239–246.

Symons, M.H., and T.J. Mitchison. 1991. Control of actin polymerization in live and permeabilized fibroblasts. *J. Cell Biol.* 114:503–513.

Takahashi, H., Y. Sekino, S. Tanaka, T. Mizui, S. Kishi, and T. Shirao. 2003. Drebrin-dependent actin clustering in dendritic filopodia governs synaptic targeting of postsynaptic density-95 and dendritic spine morphogenesis. *J. Neurosci.* 23:6586–6595.

Vartiainen, M., P.J. Ojala, P. Auvinen, J. Peränen, and P. Lappalainen. 2000. Mouse A6/twinfilin is an actin monomer-binding protein that localizes to the regions of rapid actin dynamics. *Mol. Cell. Biol.* 20:1772–1783.

Vartiainen, M.K., T. Mustonen, P.K. Mattila, P.J. Ojala, I. Thesleff, J. Partanen, and P. Lappalainen. 2002. The three mouse actin-depolymerizing factor/cofilins evolved to fulfill cell-type-specific requirements for actin dynamics. *Mol. Biol. Cell.* 13:183–194.

Wegner, A.M., C.A. Nebhan, L. Hu, D. Majumdar, K.M. Meier, A.M. Weaver, and D.J. Webb. 2008. N-WASP and the Arp2/3 complex are critical regulators of actin in the development of dendritic spines and synapses. *J. Biol. Chem.* 283:15912–15920.

Yang, C., L. Czech, S. Gerboth, S. Kojima, G. Scita, and T. Svitkina. 2007. Novel roles of formin mDia2 in lamellipodia and filopodia formation in motile cells. *PLoS Biol.* 5:e317.

Yang, E.J., J.H. Yoon, D.S. Min, and K.C. Chung. 2004. LIM kinase 1 activates cAMP-responsive element-binding protein during the neuronal differentiation of immortalized hippocampal progenitor cells. *J. Biol. Chem.* 279:8903–8910.

Zhang, H., and I.G. Macara. 2008. The PAR-6 polarity protein regulates dendritic spine morphogenesis through p190 RhoGAP and the Rho GTPase. *Dev. Cell.* 14:216–226.

Zhou, Q., K.J. Homma, and M.M. Poo. 2004. Shrinkage of dendritic spines associated with long-term depression of hippocampal synapses. *Neuron.* 44:749–757.